Title
Enhanced AHS Safety Through the Integration of Vehicle Control and Communication

Authors
Hedrick, J. K.
Sengupta, R.
Xu, Q.
et al.

Publication Date
2003

CALIFORNIA PATH PROGRAM
INSTITUTE OF TRANSPORTATION STUDIES
UNIVERSITY OF CALIFORNIA, BERKELEY

Enhanced AHS Safety Through the Integration of Vehicle Control and Communication

J.K. Hedrick, R. Sengupta, Q. Xu, Y. Kang, C. Lee
University of California, Berkeley

California PATH Research Report
UCB-ITS-PRR-2003-4

This work was performed as part of the California PATH Program of the University of California, in cooperation with the State of California Business, Transportation, and Housing Agency, Department of Transportation; and the United States Department of Transportation, Federal Highway Administration.

Report for Task Order 4210

January 2003

ISSN 1055-1425

Enhanced AHS Safety Through the Integration of Vehicle Control and Communication

Annual Report

PATH Task Order 4210

J. K. Hedrick
R. Sengupta
Q. Xu
Y. Kang
C. Lee

Mechanical Engineering Department
University of California at Berkeley
Berkeley, CA 94720

Contents

List of Figures

Chapter 1

Communication Architecture Design

In fiscal year 2002/2003 we finished the study of the effect of vehicle-vehicle/vehicle-roadside communication on the performance of adaptive cruise control (ACC) systems. Two simulation studies were finished. The first is a single ACC vehicle simulation using MATLAB/SIMULINK. A cut-in scenario and a braking scenario are tested. Communication greatly saves control effort in the former scenario, while it has little effect in the latter. The other work simulates ACC controlled highway merging using SHIFT language. The results show the beneficial effects of communication in terms of the braking effort, the waiting-to-merge queue length, and the main lane traffic shock wave caused by merging.

1.1 Introduction

In recent years a number of research efforts were conducted with the goal of enhancing the safety and efficiency of highway/urban traffic with the aid of wireless communication and modern control techniques. Both ad hoc wireless network based vehicle-vehicle (V-V) communication and infrastructure-based roadside-vehicle (R-V) communication have attracted interest from researchers in wireless communication as well as in ground transportation [1][6][10]. Aware of the great benefit such communication could bring, FCC proposed the allocation of 5.9GHz band spectrum specifically to national ground transportation safety and productivity. The on-going standardization process of

this Dedicated Short Range Communication (DSRC) band further inspires research in this field [1].

Adaptive Cruise Control (ACC) systems are the first driver control assistance systems entering the market that have the potential to influence traffic flow characteristics. In conventional cruise control the vehicle is commanded to maintain a preset velocity, regardless of the traffic environment. With adaptive cruise control, the vehicle tries to maintain a desired headway time respect to the preceding vehicle and match the preceding velocity on the basis of the measurement from forward sensors (typically millimeter wave radar or infrared laser). When V-V/R-V communication is joined with ACC, the system becomes Cooperative Adaptive Cruise Control (CACC) system. Besides the sensor measurements, CACC vehicles also receive messages communicated by the preceding vehicle and other relevant vehicles. All these vehicles cooperatively perform control maneuvers. Much work has been done to understand the effects of ACC in traffic flow [5][7][13][14]. However the CACC concept is new and the related literature is small.

We aimed to incorporate the V-V/R-V communication design and the ACC/CACC system design, and study the influence of such design on behavior of highway vehicles on both microscopic and macroscopic level. The research method we used was simulation. This choice is due to the difficulty in analytical solution of such complex systems as highway systems, and the difficulty and cost in collecting fleet of ACC/CACC vehicles to perform experiment. The simulation results could be guidelines for future analytical and experimental work.

The rest part of this chapter is organized as follows. Section 1.2 describes the key communication concepts we apply. Section 1.3 is the simulation scenario, and section 1.4 is the system modelling for the simulation. Section 1.5 reports the results of simulation and our discussion. Section 1.6 is the conclusion.

1.2 Two Communication Concepts In V-V/R-V Communication

Two specific communication concepts for V-V/R-V communication were applied in our work. However seemingly simple, they can be solutions of many challenging difficulties in V-V/R-V communication on highway.

The first one is location-based broadcast (LBB), in which the sender broadcasts a message to all the potential receivers in the communication range, and the physical location of the sender is written in the broadcast message. Each receiver determines the relevance of the message and the proper response by itself. Useful information for the sender in processing the message include the relative physical position of itself to the sender (in front, behind, left lane, how far, etc.), the nature of the message (braking, lane changing, accident, congestion, etc.), and other information in the message (velocity, acceleration, etc.). By applying LBB we avoid the difficulty of addressing and location/ communication address mapping. The realization of LBB requires sensor fusion and GPS/ INS techniques. It should be noticed that LBB only suitable for certain type of vehicle safety applications, and for some applications unicast is unavoidable.

The other concept we studied is "intermediate communication". In this kind of communication, the transmission of a message is driven by particular events, e.g. cut in, merging, braking of preceding vehicle, etc. The time-driven communication is regarded as full communication, in which vehicles transmit certain information (e.g. position, velocity, acceleration, road condition, etc.) to target receivers in every certain period of time (e.g. 100msec) [1][13]. When large number of senders are competing for the channel, as the case in V-V communication, intermediate communication can help reduce the load of channel and simplify the communication protocol design. However intermediate communication convey less information than full communication thus is not good enough for some applications. One scenario we simulated was found to be such an example.

1.3 Simulation Scenarios

Two simulation studies are reported here. The first is the simulation of the response of a single CACC vehicle to the changing highway traffic environment, and the second study simulates two highways carrying CACC vehicles that merge.

1.3.1 One-vehicle CACC simulation (OVC)

Two scenarios, Braking and Cut-in, are simulated in the OVC simulation.

In Braking scenario, two vehicles are driving in the same lane with the

follower being either an ACC or CACC vehicle. The preceding vehicle is assumed to have the capability of V-V communication when the follower is a CACC vehicle. In the simulation, the preceding vehicle brakes and the follower applies a proper braking in response to maintain the desired range and match the preceding velocity. In ACC scheme, the follower measures the range and range rate with radar and sensors. The range rate is differentiated by the on-board computer to obtain acceleration, and the braking of the preceding vehicle is detected from the change in acceleration. With V-V communication, whenever the preceding vehicle brakes, it transmits a "brake light" message to the CACC following vehicle. The CACC vehicle, upon receiving the message, brakes strongly enough for safety but not enough for passenger discomfort. Response time is increased by replacing the sensor delay and computational delay with communication delay.

In Cut-in scenario, initially an ACC/CACC vehicle is following its preceding vehicle. Then a vehicle in an adjacent lane cuts in between the two vehicles, and becomes the new preceding vehicle of the ACC/CACC vehicle. Without communication, the ACC vehicle would detect the cut-in vehicle when the latter passes the lane border. The ACC controller then commands the vehicle to brake, often abruptly, to make space in front for the cut in vehicle. With CACC system using V-V communication, the cut-in vehicle transmits the equivalent of a "turning light" message to the CACC vehicle at the instant it starts to cut in from the center of the adjacent lane. The CACC vehicle then has 2-3 seconds (half of lane change time) to slow down and make space for the cut-in vehicle.

1.3.2 Highway Merging CACC Simulation (HWC)

In HWC, vehicles merge into the main lane from a merge-in lane, and the two lanes join at a merge-in point (MP), as illustrated in Figure 1.1. Cars B and C are the main lane vehicles, and car A is in the merge-in lane.

Some or all of the main lane vehicles are ACC/CACC controlled while others are driven by humans. The percentage of the ACC/CACC vehicles in the main lane is controllable. The procedure of merge-in is as follows.

1. Head merging vehicle is generated:

   At the instant the first vehicle in the merge-in lane enters the main lane, the second vehicle in the lane becomes the new "head merging vehicle". For presentation convenience, assume car A in Fig 1.1 is

Figure 1.1: Highway Merging Scenario

the new head merging vehicle. In CACC system, at the instant it becomes the head car, A broadcasts a message to all the main lane vehicles within the communication range. The communication could be realized by either V-V communication with A being the broadcaster, or R-V communication with the aid of a roadside station close to MP. The message contains the position of the merge-in point and the time taken for vehicle A to enter the main lane. If A is driving at the instant it becomes the head merging vehicle, this time is needed for A to drive from its position at that instant to merge-in point. The distance it travels in this period of time is equal to the range between A and its old preceding vehicle, i.e. the last head merging vehicle. If A is already waiting at the merge-in point when it becomes the head, we assume a metering light at the MP commands A to wait for a certain amount of time before it attempts to merge. The benefit of this necessary waiting is evident from the simulation results.

2. Main lane vehicles process the message:

   After sending the warning message, it takes sometime for A to enter the main lane. During this period of time, each main lane vehicle determines the relevance of the received message. If a main lane vehicle C finds that at the anticipated time the head merging vehicle A arrives in the main lane, A will cut in between C and its current preceding vehicle B, it regards the message relevant. Vehicle C then brakes to increase the gap between itself and vehicle B. The response time is generally long enough for a main lane vehicle to make a "good" gap. For example, for merge-in lane flow rate of 1200 vehicle/hour/lane, the average response time is about 3 seconds. If a car finds a message irrelevant, it simply discard it. This is in accordance with the principle of location based broadcast.

3. Head merging vehicle waits for acceptable gap :

   When it arrives at the MP, the head merging vehicle stops and observes the gap between the passing vehicles in the main lane. It waits to merge in until an acceptable gap appears. If the head merging vehicle has to wait for rather long time, a queue of waiting cars will be formed in the merge-in lane.

4. Head merging vehicle merges in:

   The head vehicle merges in the gap if it feels safe. Its initial speed is equal to the main lane vehicle in front. At this instant, the main lane vehicle right behind it sees the merging vehicle, and responds by braking.

1.4 System Modelling And Design

This section describes the models implemented in the simulation and the controller design. The OVC models are implemented with MATLAB/SIMULINK software package. The HMC simulation was built using SHIFT, a language developed by California PATH for describing dynamic network of hybrid automata [2].

1.4.1 Vehicle Model

The OVC uses the vehicle model of a BMW test vehicle [9]. The model includes longitudinal vehicle dynamics, wheel dynamics, unlocked engine dynamics, torque converter model, lockup Logic, gear shifting, and the throttle/brake actuator models. Each part of the model is experimentally validated with the test vehicle in test track or urban streets. The well- studied vehicle model enables us to grasp the performance of the controller under the influence of the nonlinear dynamics of vehicle mechanical components.

In HMC, due to large number of simulated components and the complication of the scenario, we use the simple longitudinal vehicle model in (1.1) to save computation load.

$$\begin{aligned} \ddot{x}(t) &= a(t) \\ \tau\dot{a}(t) + a(t) &= u(t) \end{aligned} \tag{1.1}$$

The model composed of a double integrator and a first-order lag, where $x(t)$ and $a(t)$ are respectively the position and acceleration, and $u(t)$ is the commanded acceleration from the controller.

1.4.2 Controller Design

The ACC controller (1.2) is designed with the sliding surface technique in order to regulate the range error and range rate error.

$$a_{des}(t) = k_v\dot{r}(t) + k_p(r(t) - r_d(t)) \tag{1.2}$$

In the equation $r(t)$ and $\dot{r}(t)$ are the range and range rate, and is the desired range. The desired acceleration a_{des} is the control command, and k_v and k_p are the controller gains. Gain scheduling is used to deal with different relation of the range and range rate. The rule is that for shorter range, and more negative range rate, the controller reacts more aggressively [9]. The acceleration commanded by the controller to the vehicle is a measure of control effort. For the same level of performance on range error and range rate responses, better controller design should demand less control effort. The acceleration of the ACC/CACC controllers is bounded to -3m/s/s to 2m/s/s for safety and comfort purpose, but such limits do not apply to the human drivers.

Instead of the commonly used headway model for the desired range, we use the desired range defined by (1.3), which is a curve fitting result of human driver behavior provided by the manufacturer of the test vehicle [9].

$$r_d(t) = t_k * v^{k_0} + offset = 6.33 * v^{0.48} + 2 \tag{1.3}$$

Both in the cut-in scenario of the OVC and the HWC, whenever a CACC vehicle receives a message warning it of a vehicle cutting in front in time, it changes the desired range in the way described in (1.4).

$$\tilde{r}_d = [1 + \frac{(t - t_s)}{t_{cut\_in}}] * r_d + \frac{(t - t_s)}{t_{cut\_in}} * L \tag{1.4}$$

In the equation, r_d is the desired range defined in (1.3),$\tilde{r}_d$ is the modified desired range for the CACC controller, t_s is the instant of the receipt of the warning message, t_{cut_in} is the estimated time left for the arrival of the cut-in, and L is the vehicle length. This modified desired range means to command the controller to increase the gap to the preceding vehicle linearly with time during the time the cut-in vehicle is changing lane.

1.4.3 Other Models in HMC

In HMC, the highway is one lane, and limited access, with only passenger cars on it. The vehicle following could be controlled by either human or ACC/CACC. The human driver model is the cognitive model based on COSMODRIVE proposed by Song and Delorme [12]. Human drivers do not respond to the V-V/R-V communication messages. The lateral motion of vehicles and geometry of merge-in ramp are not modeled. Both in ACC and CACC system, merging is human controlled, because automatic controlled merging is not realizable in the near future. We use the probabilistic model of Ahmed [3] for the human decision making in merging. In this model, when seeing a good gap the driver of the merging vehicle has a higher probability to merge in, but the decision making model is probabilistic. A good gap cannot guarantee a merging, and other factors such as relative speed, distance to the point where the merging has to be completed, and delay have to be considered. In CACC, the relevant main lane vehicles try to make a more acceptable gap for the merging vehicle when it arrives, but it is human driver who makes the decision to merge or not.

1.5 Simulation Results

Figures 1.2 and 1.3 are the acceleration of the ACC vehicle and CACC vehicle in cut-in scenario of OVC. The x-axis is time in second, and y-axis is the acceleration in m/s/s. The dashed line is the desired acceleration and the solid line is the actual acceleration. The cut-in happens at 10 second for both ACC and CACC cases. The ACC vehicle detects the cut-in vehicle shortly after 10 second, and then has to apply a hard brake of -2.5 m/s/s to slow down. After this hard brake, the velocity of the ACC vehicle decreases to a safe value. The acceleration then goes back to the normal value, and finally converges to zero as the ACC goal is achieved. On the other hand, in Figure 3, because of the V-V communication, the CACC vehicle responds 2.5 seconds before the vehicle in the adjacent lane cuts in, which is half of the lane change time of the cut-in vehicle. Because the CACC vehicle has longer response time, it brakes much less than the ACC vehicle. The braking effort is smaller than 0.5 m/s/s, and the sharp time response in Figure 2 disappears. The two cases has quite similar performance on the range and range rate response, which we do not show here. Therefore the V-V communication helps save

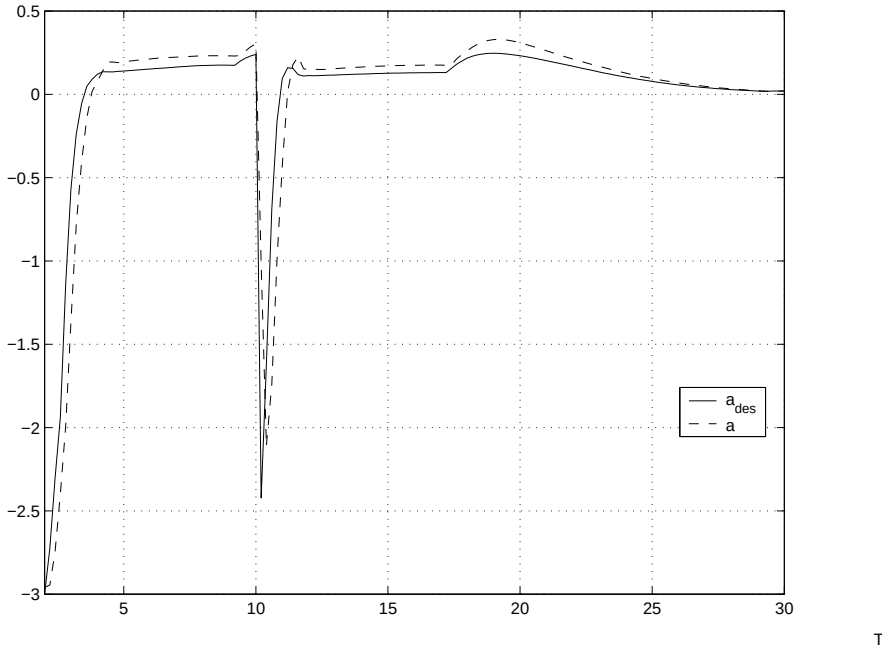

Figure 1.2: Acceleration of ACC Vehicle in OVC Cut-in Scenario

large amount of control effort, which means more safety for the vehicle, and less discomfort for the passenger.

Figure 1.4 is the range error and range rate of the ACC/CACC controller in the braking scenario of OVC. Little difference could be observed to draw clear conclusion. The control effort comparison shows the same result, which we do not show here. The reason may be that the quality of the forward sensor implemented in the simulation was quite high and the response time gained by addition of communication was not long enough for the mechanical components to yield much difference in performance. From the simulation we built, it looked that intermediate communication does not help a lot in a scenario like the braking warning.

Figures 1.5 and 1.6 are the trajectories of vehicles in the main lane between 900 second and 1000 second for ACC and CACC HMC simulation. Each curve corresponds to the trajectory of one vehicle. The x-axis is time in seconds and the y-axis is the position in meter of the vehicles. The merge-in point is at 510 meters. The horizontal line at 510 meter represents queued vehicles. Merging vehicles can be identified by a curve which lies entirely

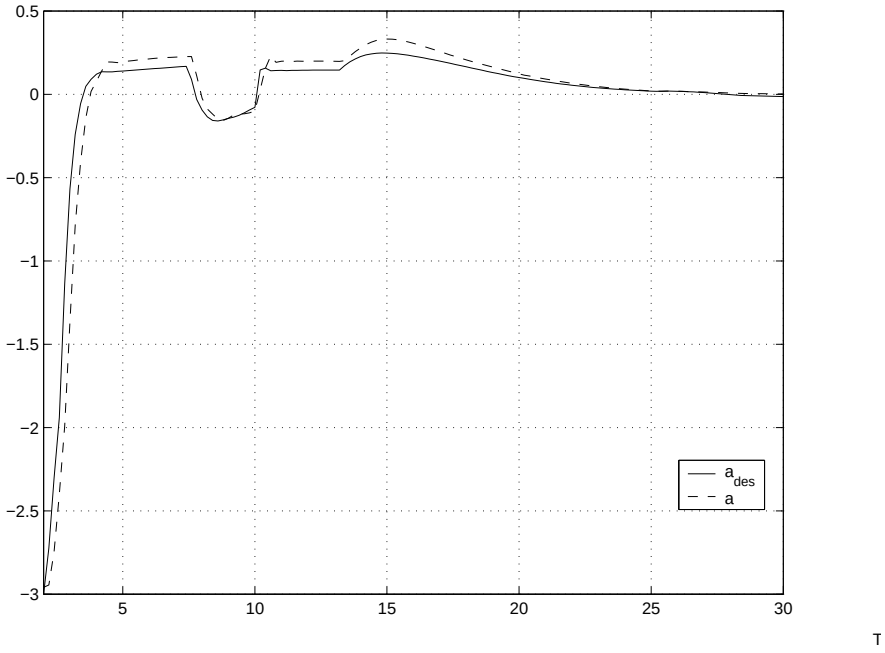

Figure 1.3: Acceleration of CACC Vehicle in OVC Cut-in Scenario

above this line. We can see clearly in Figure 1.5 a shock wave propagating upstream, i.e. in the opposite direction of the traffic. However this shock wave is smoothed in Figure 1.6. The reason lies in two facts. First is that the relevant main lane vehicle receives the warning message well in advance, thus it can brake smoothly to make the gap to preceding larger. Second is when the merging vehicle enters the main lane, the gap it is in is already large enough for safety, and the main lane vehicles behind it do not need to brake hard, as they have to do in ACC highway.

We repeated the simulation with various market penetration of the ACC (CACC) vehicle. Figures 1.7 and 1.8 summarize the market penetration effect in braking effort. In Figure 1.7, the "mean maximum braking effort" vs. percentage of ACC (CACC) vehicle is shown. In the duration of simulation each vehicle has a maximum braking effort. The mean maximum braking effort is the average, over all vehicles appearing in the simulation, of the vehicle's maximum braking effort. It was used as a measure of the average braking effort of all vehicles. In the figure the solid line stands for the CACC case, and the dashed line stands for the ACC case. Evidently we can see

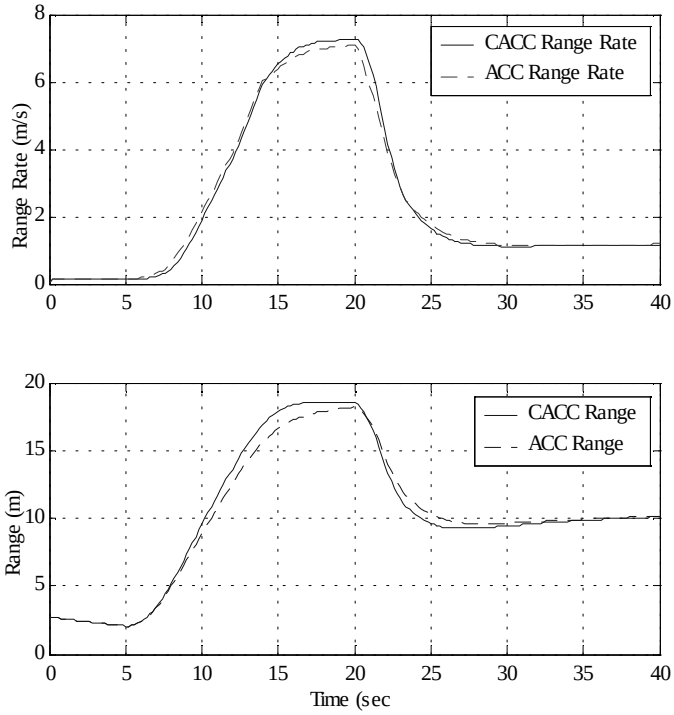

Figure 1.4: Range and Range Rate in OVC: Braking Scenario

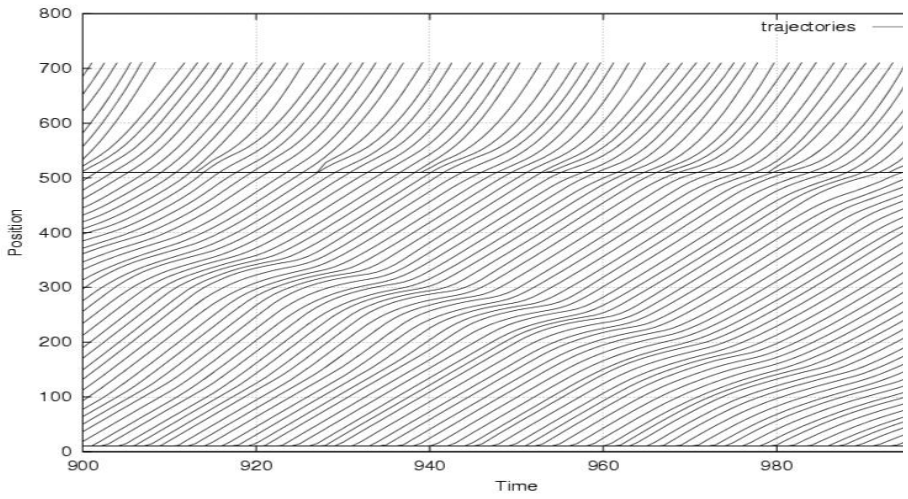

Figure 1.5: Trajectories of Main Lane Vehicles in ACC Highway Merging

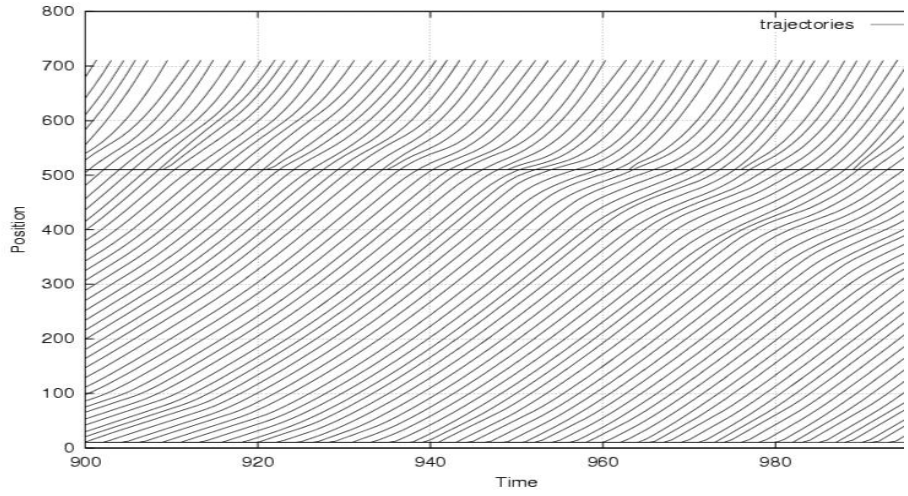

Figure 1.6: Trajectories of Main Lane Vehicles in CACC Highway Merging

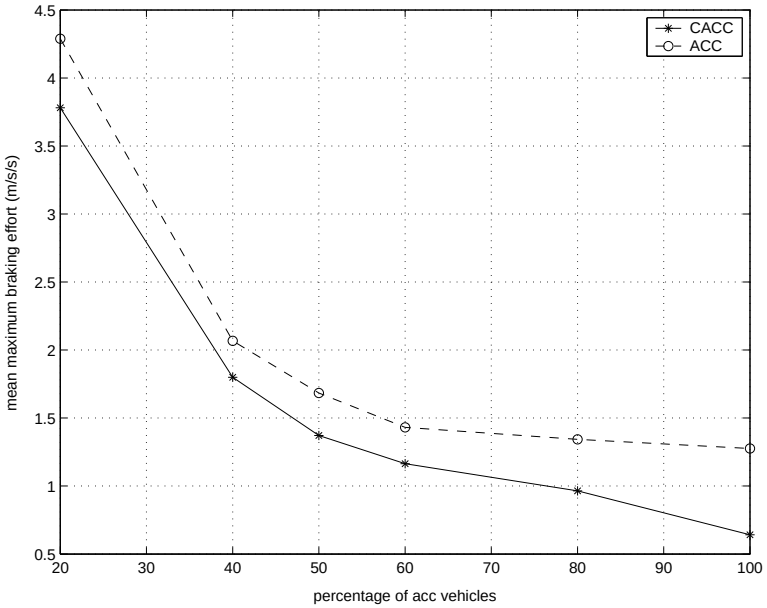

Figure 1.7: Average Braking Efforts for Different Market Penetration of ACC/CACC Vehicles in HMC

the following facts. The more ACC vehicles in the highway, the smaller the average braking effort is. With the same percentage of ACC vehicles, CACC performs better than ACC in saving the braking effort. This result is consistent with those of cut-in scenario of OVC, due to the similarity of merge-in and cut-in.

Figure 1.8 shows the length of the queue of the waiting to merge vehicles in the merge-in lane from 600 to 1000 second. Results for four cases are plotted here. In the two mixed cases the rest of the vehicles are human driven. The top curve is for 50% ACC main lane vehicles. In the middle, two curves standing for 100% ACC and 50% CACC are quite close to each other. The bottom curve is for 100% CACC. The queue length keeps increasing because we intentionally inject large enough input flow over the capacity of the highway. Clearly, the larger the percentage of ACC (CACC) vehicles, the shorter the waiting queue. For the same percentage, the queue in CACC highway is up to 5 vehicles shorter than in ACC highway. Due to the communication, the relevant main lane vehicles have longer time to make a good gap in front. By the time the merging vehicle arrives at MP, it is more likely to

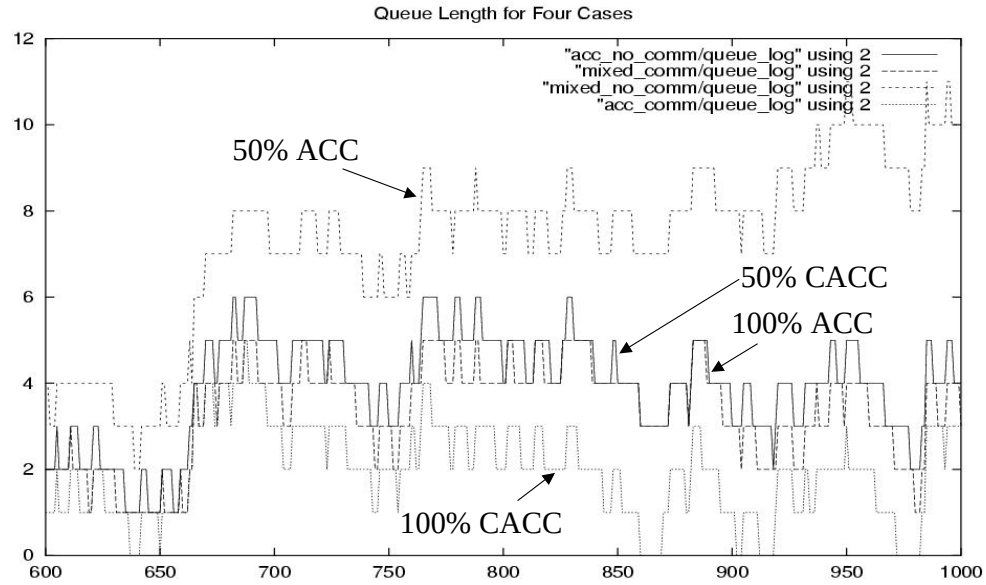

Figure 1.8: Queue Length of Waiting-for-Merge Vehicles in HMC

see an acceptable gap and merge in than reject the gap and wait. Therefore in average the merging cars wait shorter in CACC highway, and the queue behind it is shorter.

1.6 Summary

In conclusion, for the types of ACC applications we studied, V-V/V-R communication brings great benefits. The benefits can be observed in terms of efficiency (waiting-to-merge queue length), safety (shock wave, braking effort, etc.) and passenger's comfort (braking efforts). Simple communication concepts like location based broadcasting and intermediate communication could work very well in these applications. But for some applications such effects are not obvious. The simulation works can serve as the guideline for further experimental work. For example, the braking scenario and similar applications should not be the focus of future experiment. Besides the experiments, how to design protocol to realize such communication with high Qos, and low cost is another direction of future work.

Chapter 2

Emergency Braking Maneuvers

2.1 Introduction

Traditionally the control strategy in an emergency situation has been to bring a vehicle to a stop as quickly as possible. This is the motivation behind such concepts as anti-lock brake systems(ABS). However, in an Automated Highway System, traffic is organized into platoons with relatively small distances. The platoon must ensure that the vehicles will not collide each other even if the platoon ahead of it brakes abruptly. There have been several research efforts in PATH dealing with emergency braking of the platoon. Alvarez and Horowitz used a collision-free notion of safety to design de-coupled platoon maneuvers in the case when platoons have different braking capabilities in [4]. Under MOU 319, the vehicle motion and collision is modelled as a hybrid system and the safety conditions under certain deceleration strategies are suggested [8] [11]. In this project, a slip-based brake controller capable of performing under high-slip conditions is proposed which will reduce the tracking errors induced by the the excessive force.

Nonlinear sliding mode control has proven effective in addressing the nonlinearities and parametric uncertainties associated with vehicle control. This strategy has been working very well under normal driving conditions. However, the problem with this approach, and vehicle control in general, is that the control inputs of the engine and brake torque enter in at the wheel, while it is ultimately desired to control the motion of the vehicle as a whole. In order to relate the desired vehicle dynamics to desired wheel dynamics, a limited slip assumption is applied. This is based on the familiar kinematic

relationship between linear(v) and angular velocity(ω) under rolling without slip:

$$v = r\omega \tag{2.1}$$

While under normal driving this assumption is reasonable, it does not hold under hard braking or acceleration. In order to overcome this limitation, a brake controller that uses the empirical relationship between road force and wheel slip to relate the wheel dynamics to the vehicle dynamics has been suggested and evaluated. Theoretically, a new controller can compensate for the errors accumulated from the limited slip assumption and improve the braking performance. In this chapter, a controller with a limited slip assumption and a slip-based controller are introduced. Then, the simulation results of the two controllers are presented. Also, the experiments of an emergency braking maneuver are executed and the characteristic behaviors of a vehicle under emergency braking are analyzed.

2.2 Control Methods for the Emergency Braking

In this project, a new control method based on the idea of using tire slip data for the precise control of the vehicle longitudinal motion is developed. Typical behavior of an emergency braking maneuver can be characterized by a rapid deceleration which will induce a large amount of slip in the tire. In such a situation, the limited slip assumption on which previous nonlinear longitudinal vehicle control is based is not valid. We will analyze the performance and availability of a new slip-based controller and compare it with those of nonlinear control methods based on the limited slip assumption.

2.2.1 Controller with Limited Slip Assumption

In this section, a simplified model of the vehicle dynamics for control purposes is described. It is assumed that the torque converter is locked, therefore the dynamics of the torque converter are neglected.

In the vehicle system there are two levels of dynamics that we are concerned with. One level is the dynamics of the vehicle as a whole, and the other is the dynamics of the wheels. The dynamics are represented by

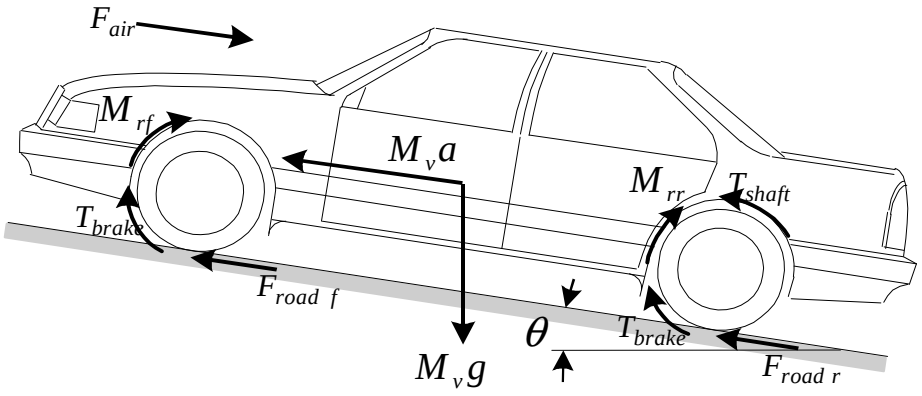

Figure 2.1: Vehicle System Dynamics.

$$M_v \dot{v} = F_{road} - F_{roll} - F_{air} - \Delta f_1 \tag{2.2}$$

$$J_w \dot{\omega} = T_{shaft} - T_{brake} - hF_{road} - \Delta f_2. \tag{2.3}$$

M_v represents the mass of the vehicle, J_w the rotational inertia of the wheel, and h denotes the effective radius of the wheel. Δf_1 and Δf_2 denote the modelling uncertainty. Road grade is omitted in the analysis for simplicity.

In practice, aerodynamic drag force (F_{air})is usually expressed in the following form:

$$F_{air} = C_d v^2 \tag{2.4}$$

which is proportional to the square of vehicle speed.

The rolling resistance(F_{roll}) of the tire is primarily caused by the hysteresis in tire materials due to the deflection of the carcass while rolling. Based on experimental results many empirical formulas have been proposed for calculating the rolling resistance of the tires. In this project, aerodynamic friction is ignored, and the rolling resistance is assumed to be constant over the entire operating region.

Table 2.1 summarizes the vehicle parameters used for all the simulations. These parameters were obtained from those of the experimental vehicle used by PATH, and this vehicle is used to experimentally verify the suggested control algorithm.

Mass (M_v)	2000 Kg
Wheel moment of inertia (J_w)	1.93 Kg/m^2
Aerodynamic drag coefficient (C_d)	0.53
Wheel effective radius (h)	0.33 m
Rolling resistance (F_{roll})	172 N
Engine inertia (J_e)	0.2630 Kg/m^2
Gear ratio	[0.4167, 0.6817, 1.0, 1.4993]
Final drive ratio	0.3058

Table 2.1: Vehicle Parameters

To control the longitudinal motion of the vehicle, a nonlinear control method called 'Dynamic Surface Control' is used. Dynamic surface control is a method which avoids the explosion of terms when designing a multiple sliding surface controller. Also this controller holds the robustness property which is one of the typical characteristics of most nonlinear controllers. We assume the vehicle dynamics and wheel dynamics described in equation 2.2 and 2.3, are related by

$$v = h\omega. \tag{2.5}$$

Then, we have the following combined equation.

$$\dot{v} = \frac{1}{\beta}\{T_{net} - h(F_{air} + F_{roll} + \Delta f_1) - \Delta f_2\} \tag{2.6}$$

where T_{net} and β are represented by

$$T_{net} = (\frac{T_e}{R_g} - T_b) \tag{2.7}$$

and

$$\beta = (M_v h + \frac{4J_w}{h} + \frac{J_e}{hR_g^2}) \tag{2.8}$$

where J_e denotes the engine inertia. R_g represents the combined coefficient of gear ratio and final drive ratio so that equation 2.9 holds.

$$\omega_e = \frac{\omega}{R_g}. \tag{2.9}$$

The control objective of the longitudinal vehicle motion is tracking a desired velocity profile while maintaining a desired level of spacing with the

vehicle it is following. To describe this control goal, a sliding surface S is defined in terms of the spacing error(ϵ) between the preceding and following vehicle.

$$S = \dot{\epsilon} + \lambda\epsilon. \tag{2.10}$$

Taking the derivative of our surface S_1, we get

$$\dot{S} = \ddot{\epsilon} + \lambda\dot{\epsilon} = (a_{des} - a) + \lambda(v_{des} - v). \tag{2.11}$$

If the control input is defined so that it tries to push the defined surface S to zero, then according to this equation 2.11, ϵ will also asymptotically converge to zero. This can be accomplished if we choose the control input to make the Lyapunov function defined below, satisfy the stability condition.

$$V = \frac{1}{2}S^2 \tag{2.12}$$

This quadratic form of the Lyapunov function is positive definite, and if our control input makes $\dot{S} = -\eta S$, then $\dot{V} = -\eta S^2$ is negative definite, therefore our Lyapunov function satisfies the asymptotic stability conditions.

Assuming a linear relation between brake pressure and brake torque of $T_b = K_b P_w$ the control input satisfying those stability conditions are as follows.

$$P_{w\,des} = \frac{1}{K_b}\Big[\frac{T_e}{R_g} - h(F_{air} + F_{roll} + \Delta f_1) - \Delta f_2 - \beta\{a_{des} - \lambda(v - v_{des}) + \eta S\}\Big] \tag{2.13}$$

If we have the control gain η large enough to overcome the model uncertainty, then the above control law will have the desired robustness property, but a large control gain is not desired from the optimal point of view. In practical applications, it is difficult to know how much uncertainty we have, so the control gain is tuned by trial and error.

2.2.2 Slip-based Controller

In the control algorithm suggested above, the wheel dynamics and vehicle dynamics are combined into one equation using the assumption that vehicle speed is the multiplication of wheel effective radius and wheel rotational speed. This assumption is valid as long as we have small traction forces

acting on the tire. However, as the vehicle accelerates or decelerates, the gap between vehicle speed and the multiplication of wheel radius and rotational speed increases because of the heavier traction force. Hence, to quantify those differences, slip is defined as equation 2.14.

$$s = \frac{r\omega - V}{max(r\omega, V)} \tag{2.14}$$

When driving torque is applied, the tire rotates without the equivalent translatory progression, therefore, $r\omega > V$ and a positive value for slip results. When braking torque is applied instead, $r\omega < V$ and a negative value for slip results. Many theories deal with this relationship between the road force and tire slip, and the Bakker-Pacejka 'Magic Tire Formula' of the form in equation 2.15 is employed in this study.

$$s = D\sin(C\arctan[B(s+S_h) - E(B(s+S_h) - \arctan(B(s+S_h)))]) \tag{2.15}$$

The fundamental idea behind the design of a slip-based controller is that we can use the above empirical relationship between road force and slip. Then, we don't need to combine the vehicle and wheel dynamics, assuming that the vehicle speed and the multiplication of wheel radius and rotational speed are the same. Each dynamic equation can be solved by applying the tractive force calculated from the above magic tire formula to get a more precise control law suitable for an emergency braking maneuver.

The first step in the design of this controller is to define the sliding surface. The first surface dealing with space tracking is identical with the previous control method described in equation 2.10. But instead of using the combined equation of vehicle and wheel dynamics, vehicle dynamics equation 2.2 is substituted into equation 2.11 to get the following equation.

$$\dot{S}_1 = a_{des} - \frac{1}{M}(F_{road} - F_{air} - F_{roll} - \Delta f_1) + \lambda(v_{des} - v) \tag{2.16}$$

Choosing a synthetic input(v_1) as F_{road}, the synthetic input should have the following value to make the first surface stable.

$$v_1 = M\{a_{des} + \lambda(v_{des} - v) + \eta_1 S_1\} + F_{air} + F_{roll} + \Delta f_1 \tag{2.17}$$

The second surface is defined as,

$$S_2 = v_1 - v_{1\,des}. \tag{2.18}$$

For this second surface we don't want to take the derivative of the desired road force because that information is unknown, therefore the technique of the dynamic surface control is employed. The filtered value is defined in equation 2.19.

$$\tau_2 \dot{v}_{1\,des\,filt} + v_{1\,des\,filt} = v_{1\,des} \tag{2.19}$$

By choosing tau_2 sufficiently small, the lag due to the filter will be minimized, and this approximation becomes reasonable.

Then the derivative of the first surface is described as,

$$\dot{S}_2 = \dot{v}_1 - \dot{v}_{1\,des} \approx \dot{F}_{road} - \dot{v}_{1\,des\,filt}. \tag{2.20}$$

Next, taking the derivative of the road force at each wheel makes the wheel dynamics appear.

$$\dot{F}_{road} = \sum \frac{\partial f_i}{\partial s_i} \dot{s}_i = \sum \frac{\partial f_i}{\partial s_i} \left(\frac{r_i \dot{\omega}_i}{V} - \frac{r_i \omega_i \dot{V}}{V^2}\right) \tag{2.21}$$

Substituting the wheel dynamics and the vehicle dynamics from equation 2.3 and 2.2, one can see that our control input, master cylinder pressure, now has access to our states through the brake pressure at the wheel. The final control input on the master cylinder pressure is expressed in equation 2.22,

$$\begin{aligned} P_w \;=\; & \{\sum \frac{\partial f_i}{\partial s_i} \frac{h_i b_i K_b}{J_w + a_i \frac{J_e}{R_g^2}}\}^{-1} \Big[\sum \frac{\partial f_i}{\partial s_i} \frac{h_i (h_i a_i T_e - h_i f_i - \Delta f_2)}{J_w + a_i \frac{J_e}{R_g^2}} \\ & - \sum \frac{\partial f_i}{\partial s_i} \frac{h_i w_i}{M_v v} (\sum f_i - F_{air} - F_{roll} - \Delta f_1) - v(\frac{v_{1\,des} - v_{1\,des\,filt}}{\tau_2} \\ & - \eta_2 S_2) \Big] \end{aligned} \tag{2.22}$$

where a_i and b_i represents the ratio of shaft and brake torque distributed to each wheel, and $\sum$ denotes the summation over all four wheels.

2.2.3 Simulation Results

The desired velocity profile command to the controller is shown in figure 2.2, where the deceleration is set to be $-7m/s^2$. This deceleration is almost the maximum rate of velocity which our experimental vehicle can follow without locking its wheels. It is assumed that in an emergency situation, vehicles in

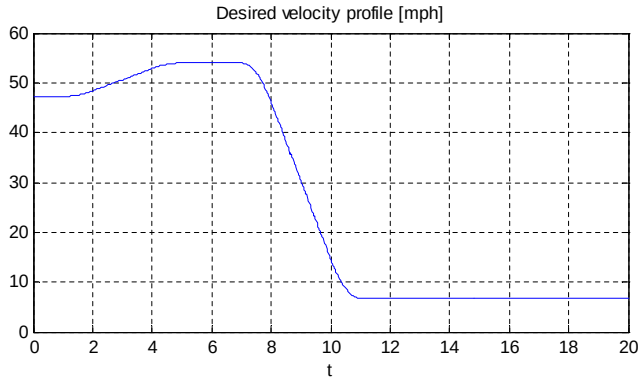

Figure 2.2: Desired Velocity Profile.

the platoon will try to follow a certain desired velocity profile decelerating as fast as they can. Also the designed controllers are assumed to have the exact modelling parameters of the vehicle. However, even with some modelling or parameter uncertainties, both nonlinear controllers showed nice robustness properties in the simulation result.

In an automated highway system the inter-vehicle spacing is expected to be very small to increase the road capacity of the traffic. Therefore, space tracking errors should be minimized for the vehicles in a platoon to avoid collision during emergency braking. Figure 2.3 (a) and (b) shows the space tracking error of the two controllers during the simulation. It is observed that the maximum space tracking error of the slip-based control is smaller than that of the limited slip controller. According to this results, the vehicles controlled by the developed slip-based controller is expected to have a smaller chance of collision during the emergency braking maneuver.

Figure 2.3 (c) and (d) shows the slip generated on the tire during the simulation. Excluding the peak values of impulsive slip change, the maximum slip occurs around 0.04 which is quite large with the tire model we used. This is because the maximum friction coefficient of the experimental vehicle is found near the slip of 0.05 in normal driving condition.

We can conclude that the slip-based controller reduced the tracking error and improved the control performance slightly. However, the simulation results do not show a significant performance improvement. This is because our simulation is limited to the -0.05–0.05 slip range, and this is not an enough slip to break the limited slip assumption. The concept of slip-based control is proposed because of the significant amount of slip that will be generated

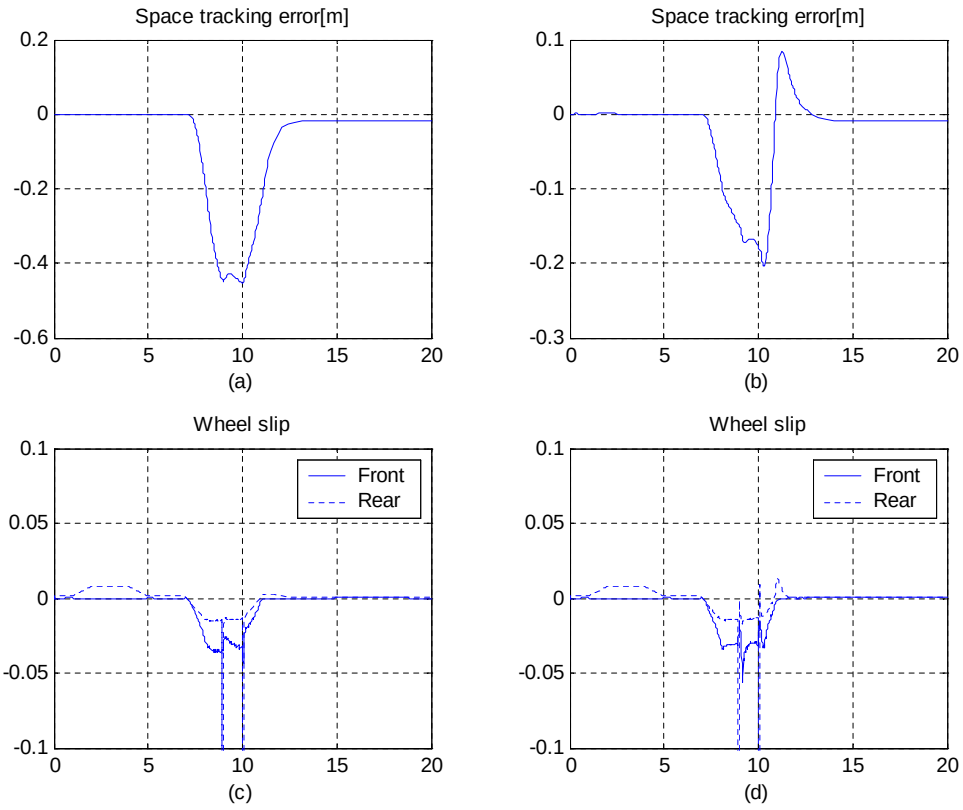

Figure 2.3: (Using stiff tire model)(a) Space tracking error of the controller assuming limited slip. (b) Space tracking error of the slip-based controller. (c) Slip on each wheel with the controller assuming limited slip. (d) Slip on each wheel with the slip-based controller.

during an emergency braking situation. However, as long as vehicles are equipped with anti-lock braking systems, the slip will not go beyond the value of the maximum friction coefficient, hence the limited slip assumption is still valid. Besides the limitation on slip due to the anti-lock brake systems, it is undesirable for the vehicle to have a large amount of slip because the excessive slip will make the wheels lock and cause the vehicle to be unstable and lose maneuverability. Using the slip data for control will not be worth the expense of the complex calculation and the risk of introducing slip measurement noise as long as the controller limited slip assumption holds and the controller is robust enough to handle the errors caused by the assumption. From the above simulation results, it is assured that the existing controller has enough performance even in an emergency braking situation and in the next chapter it will be verified experimentally.

2.3 Experimental Testing of Emergency Braking

Vehicles equipped with the necessary sensors and actuators are used to experimentally verify the performance of the controller designed in this project. Simulations provided a qualitative understanding of controller performance. However, performance in a real world environment still has to be assessed.

The simulation results of section 2.2 showed that the both of the controllers will track the desired longitudinal motion without causing too much tracking error during emergency braking. Hence, we made an experiment with the controller assuming limited slip only, and the performance of the controller in a real situation is checked.

The emergency maneuver of the vehicle on the dry and wet surface is tested and the problems of applying current control strategy to the emergency braking is analyzed.

2.3.1 Experimental Setup

All of the experimental work was performed on the Red Lincoln Towncar provided by California PATH. The actuators on the vehicle consist of a stepper motor on the throttle valve, and pump accumulator system that generates hydraulic pressure to actuate the vehicle's master cylinder. It should be

noted that the brake actuator has been characterized as having a 30 msec pure time delay, as well as a first order lag of 20 msec.

Wheel rotational speed sensors implemented on the experimental vehicle output two signals: one optimized for low speed and the other for high speed. Vehicle velocity is measured by the extra 5th wheel contacting the road surface and rolling freely with constant radius. By counting the teeth of gears on the wheel for a constant period, vehicle velocity can be estimated. Brake pressure sensor at the wheel and master cylinder is determined from pressure transducers.

The control code for this vehicle is implemented in C on a Pentium processor running the QNX operating system. The C code for the QNX computer is automatically generated using the Real-Time Workshop toolbox of MATLAB from a Simulink file composed of data input and output ports, data processing blocks, and controller blocks. This procedure enables us to directly implement the controller used in the simulation to the experimental vehicle.

2.3.2 Controller Performance

The experiment was performed on the track in Richmond Field Station, and the desired velocity profile commanded to the controller is shown in figure 2.4. The vehicle could not be driven as fast as it is in the simulation due to the speed limit on the test track, so the deceleration was maintained only for a short period.

For the first 7 seconds, the vehicle is commanded to maintain a constant speed because we want each result to have the same initial condition before braking so that the clear effect of the emergency braking can be shown. Then, the vehicle is commanded to decelerate as fast as -8 m/s^2 until it stops. The same test was performed on the dry surface and wet surface to observe the effect of the different friction coefficient on the control performance.

In figure 2.5 (a) the space tracking errors on the dry and wet surface are plotted. Similar to the simulation results, the errors increase as the deceleration proceeds. However, due to the modelling or parameter uncertainty, more errors are measured than were shown in the simulation results.

Negative space tracking errors imply that the inter-vehicle distance has been reduced and as long as the maximum errors are lower than the inter-vehicle spacing, a collision will not occur.

In the figure 2.5 (b) the gap between the actual velocity and desired

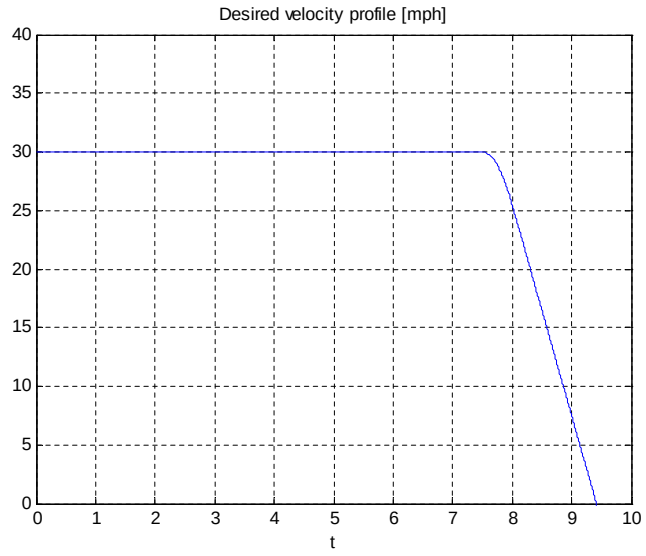

Figure 2.4: Velocity Profile of the Experimental Vehicle

velocity is larger on the wet road than on the dry road because of the limited availability of the friction force on the wet road.

2.3.3 Emergency Braking Vehicle Behavior

In figure 2.6, the wheel speed and the slip generated during the test is plotted. It is observed that as the errors increase during the braking, more control efforts are applied to compensate for the errors, and the slip increases as error to make the wheels lock. These results are not observed on the dry road, but obvious on the wet road. In figure 2.6 (b) and (d), the front wheels almost lock making the slip as small as -0.5.

If the controller eventually makes the wheels lock when the friction coefficients are low, it may not be a good control strategy for an emergency braking situation. The maximum friction coefficient estimation technique will help to avoid such a situation. Also the cooperative control strategies can be beneficial to avoid rear-end collision of the platoon.

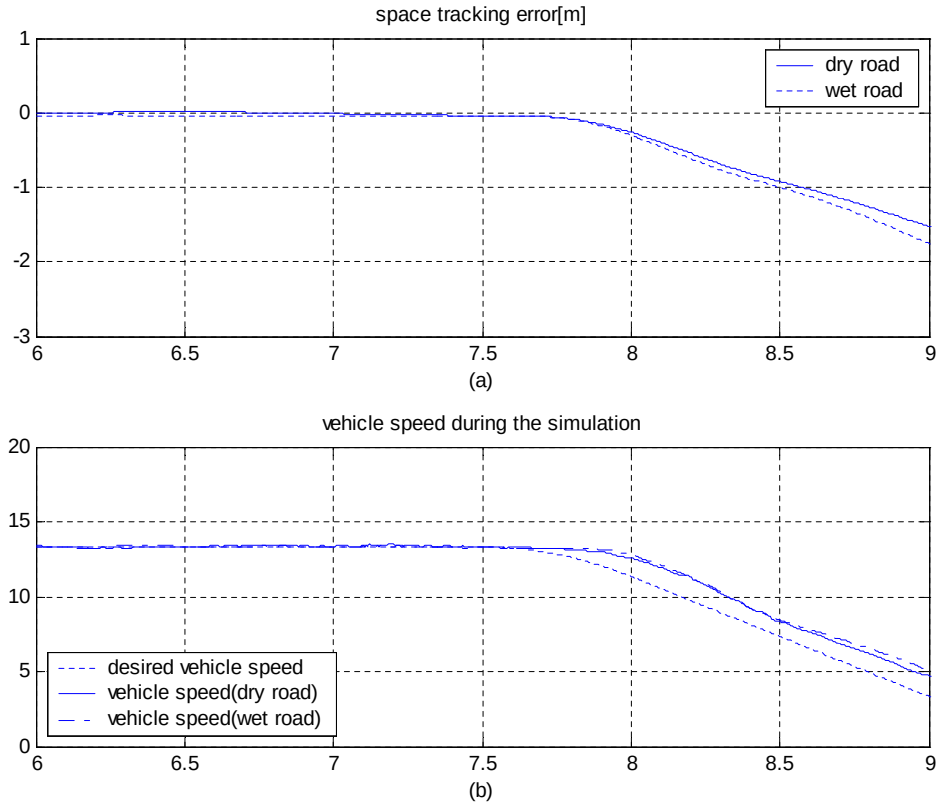

Figure 2.5: (a) Space tracking error on the dry and wet road (b) Velocity profile on the dry and wet road

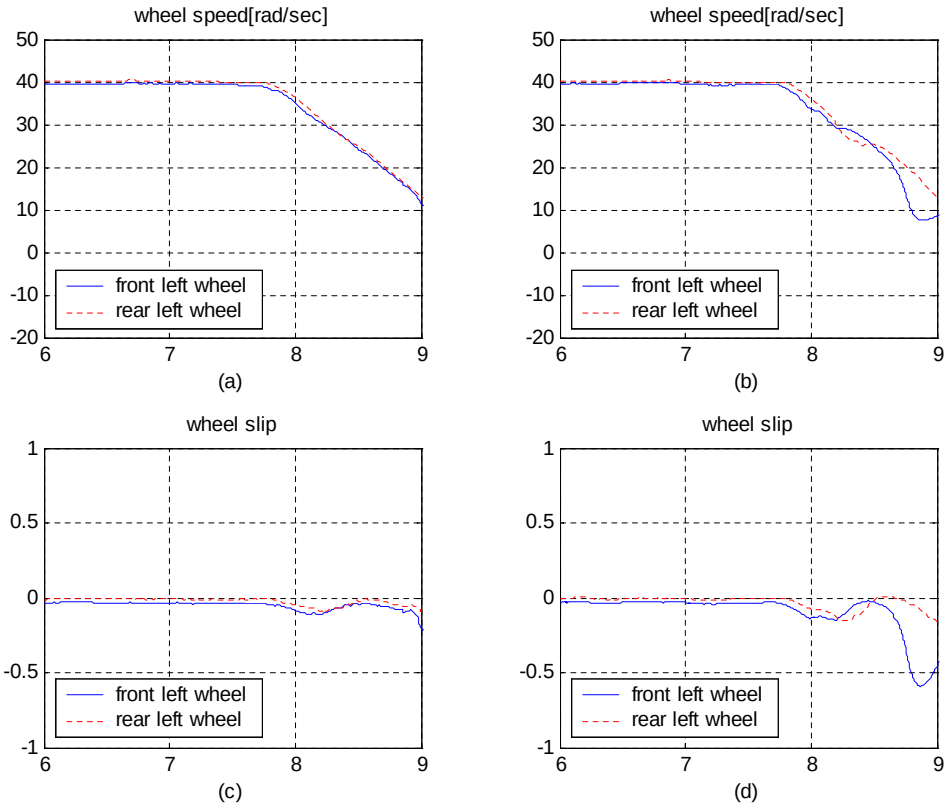

Figure 2.6: (a) Wheel speed on the dry surface (b) Wheel speed on the wet surface (c) Wheel slip on the dry surface (d) Wheel slip on the wet surface

Chapter 3

Slip-based Road Condition Estimation

3.1 Introduction

Many reports have introduced an algorithm to determine the road's frictional characteristics. However, this research focuses on obtaining the maximum braking performance of a car by using the maximum friction coefficient, μ_{max}, which can be estimated using the slip of a wheel. In other words, given the current road condition, it is important to know which way and how fast a car can be stopped without vehicle skidily. One easy way to determine when vehicle skid occurs is to calculate the maximum friction coefficient. The μ_{max} between the road and the tire can be obtained using Equation 3.1.

$$\mu = \frac{\sqrt{F_x^2 + F_y^2}}{N_z} \tag{3.1}$$

The F_x, F_y, N_z in this equation are longitudinal, lateral, normal force applied on the tire, respectively. In this report, F_y can be disregarded since only the longitudinal motion of a vehicle is considered, and lateral motion has been ignored. Therefore, Equation 3.1 can be simplified as shown in Equation 3.2

$$\mu = \frac{F_x}{N_z} \tag{3.2}$$

In Equation 3.2, the maximum friction coefficient is $\mu_{max} = \max|\mu| =$

$\max|\frac{F_x}{N_z}|$. Therefore, the normal force and maximum longitudinal force applied to a tire are known, the maximum friction coefficient can be easily obtained. By using the relationship between the maximum friction coefficient and the maximum acceleration of a car, Equation 3.3 can be derived.

$$\begin{aligned} |a_x|_{max} &= \max|\frac{F_{x11}+F_{x12}+F_{x21}+F_{x22}}{m}| = \max|\frac{\mu N_s}{m}| \\ &= \max|\frac{\mu mg}{m}| \leq \mu_{max} g \end{aligned} \tag{3.3}$$

In Equation 3.3, g is the gravitational constant, and m is the total mass of a vehicle. Therefore, the maximum acceleration of a vehicle, while it is in motion, can be determined by estimating μ_{max}. For ABS(Anti lock Brake System), TCS(Traction Control System)or VDC(Vehicle Dynamics Control system), it is not possible to increase the maximum acceleration limit even though such systems are operated when a driver needs acceleration or deceleration that exceeds μ_{max}.

However, a μ_{max} estimator provides in real time the information to a human or machine driver that can prevents emergency situation. Hence, not only does it provides improvement in safety, but also it increases the efficiency of Vehicle Distance Control System.

Figure 3.1 shows the well known relationship between the longitudinal slip ratio of a tire and friction coefficient(Normalized longitudinal force). When slip increases, normalized longitudinal force also increases; however, after reaching the maximum value, normalized longitudinal force gradually declines. As for the braking condition, when the brake pressure is increased and exceeds the certain pressure, the slip of a wheel excessively occurs and the longitudinal force gradually decreased. Therefore, this research will estimate the maximum friction coefficient on the basis of this relationship shown in Figure 3.1.

Slip on each wheel is the difference between the circumferential velocity of a wheel and translational velocity of a vehicle, and the definition of slip used in this research is shown in Equation (4).

$$s = \frac{r\omega - v}{\max(r\omega, v)} \tag{3.4}$$

v in Equation 3.4 is longitudinal velocity, ω is angular velocity of a wheel, and r is the tire effective radius. In order to obtain the relationship between

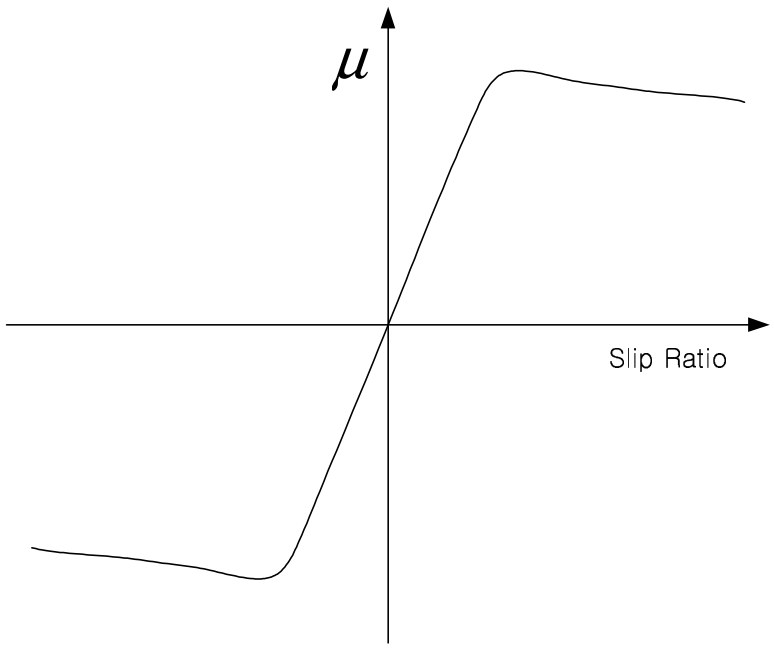

Figure 3.1: Longitudinal Slip Ratio Vs. Friction Coefficient.

slip and friction coefficient, Normal Force Estimator, Tire Effective Radius Estimator, Road Force Estimator are used. Also, a speed sensor is attached to each wheel, and the Fifth Wheel, which has almost zero slip, is attached to the rear bumper of the vehicle to measure the velocity.

3.2 Vehicle Speed and Wheel Speed Detection

On each wheel, Magnetic Pulse Detector is attached, and the angular velocity of a wheel can be measured with the series of magnetic pulse. However, the magnetic pulse contains lots of noise, and Kalman Filter is used to filter noise.

$$\begin{bmatrix} \dot{x_1} \\ \dot{x_2} \end{bmatrix} = \begin{bmatrix} 0 & 1 \\ 0 & 0 \end{bmatrix} \begin{bmatrix} x_1 \\ x_2 \end{bmatrix} + \begin{bmatrix} 0 \\ 1 \end{bmatrix} \omega \tag{3.5}$$

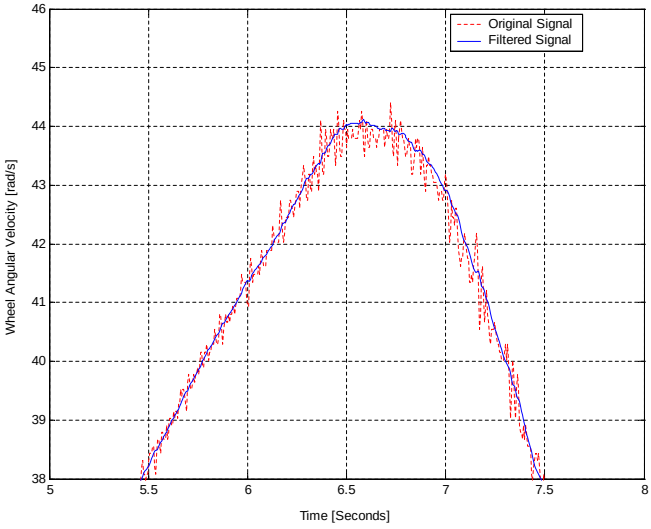

Figure 3.2: Wheel Angular Velocity Signal

$$y = \begin{bmatrix} 1 & 0 \end{bmatrix} \begin{bmatrix} x_1 \\ x_2 \end{bmatrix} + v \tag{3.6}$$

x_1, x_2 are angular velocity and angular acceleration of a wheel, and ω, v represents system disturbance and sensor noise, respectively.

$$\dot{\hat{x}} = A\hat{x} + L(y - \hat{y}) = (A - LC)\hat{x} + Ly \tag{3.7}$$

$$\dot{\hat{x}} = \begin{bmatrix} L_1(x_1 - \hat{x}_1) + \hat{x}_2 \\ L_2(x_1 - \hat{x}_1) \end{bmatrix} \tag{3.8}$$

L_1 and L_2 are Kalman filter gain.

Figure 3.2 shows the comparison between the original signal and the filtered signal.

Using Magnetic Detector the number of teeth on Fifth Wheel over a certain amount of time is measured. With the result and through the magnetic signal process shown in Figure 3.4, the velocity of the vehicle can be measured.

Figure 3.5 shows the actual velocity and filtered velocity, which uses Low Pass Filter.

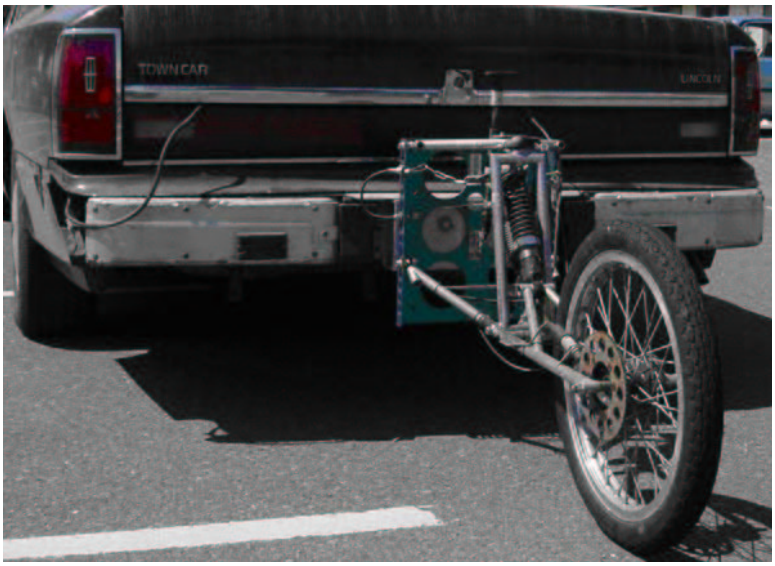

Figure 3.3: Fifth Wheel

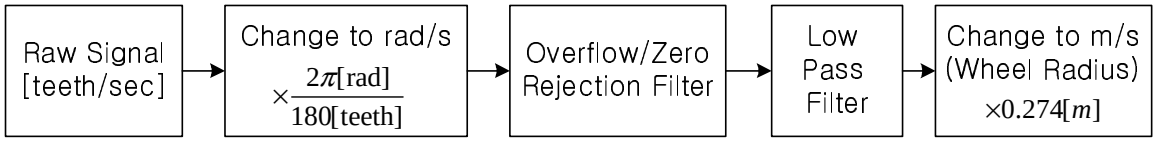

Figure 3.4: Velocity Detection Procedure

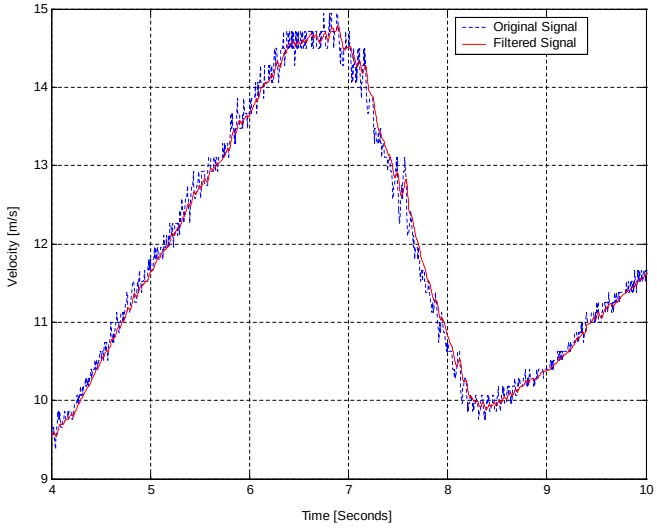

Figure 3.5: Velocity Signal Filtering using Low Pass Filter

3.3 Normal Force Estimator

To obtain the friction coefficient between road and a tire, normal force applied on each wheel needs to be calculated. Also, the exact circumference of each tire is needed to measure the exact slip. The circumference of each tire is exceptionally important to be measured because it is influenced by normal force a lot. Two ways are used to observe normal force on each tire: "Static Normal Force Estimator" which analyzes the vehicle statically and "Dynamic Normal Force Estimator" which considers both suspension and pitch motion. Figure 3.6 shows the model for Static Normal Force Estimator, and normal forces applied on front and rear wheels are represented in Equation 3.9. Figure 3.7 shows Dynamic Normal Force Model which includes suspension and tires. Using dynamic equations, normal forces applied on all four wheels are shown in Equation 3.10.

$$N_f = \frac{mgl_r - mah}{l_f + l_r}, \quad N_r = mg - N_f \tag{3.9}$$

$$\begin{aligned} F_{nf} &= 2k_{tf}R_u - (h_f + z_{uf}) \\ F_{nr} &= 2k_{tf}R_u - (h_r + z_{ur}) \end{aligned} \tag{3.10}$$

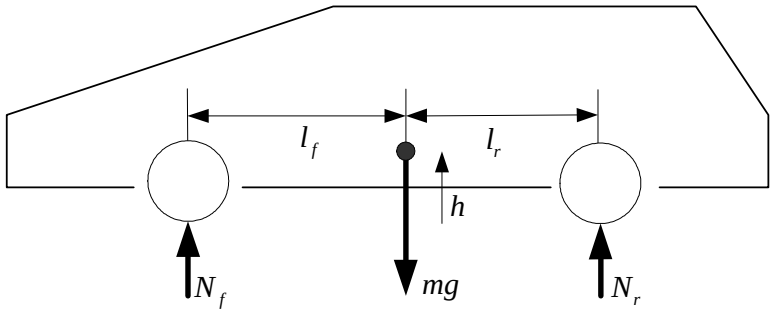

Figure 3.6: Static Normal Force Model

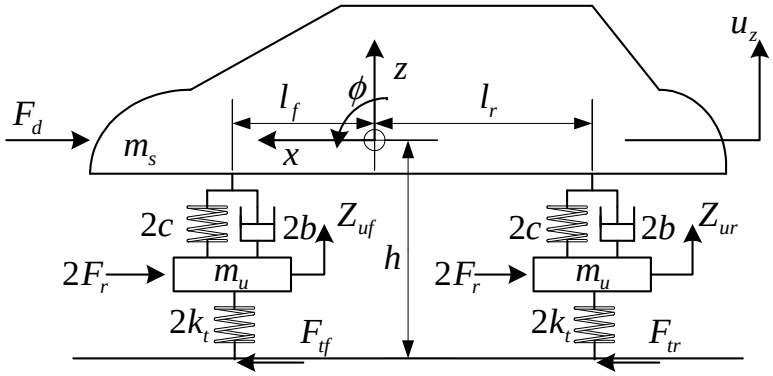

Figure 3.7: Dynamic Normal Force Model

Figure 3.9 and 3.10 shows the normal force applied on wheels using static/dynamic normal force estimator supposing the vehicle has the same velocity profile shown in Figure 3.8. As shown in Figure 3.9 and 3.10, static normal force and dynamic normal force have a similar value. Hence, in an attempt to lessen the calculation load of the system, the static normal force estimator is used.

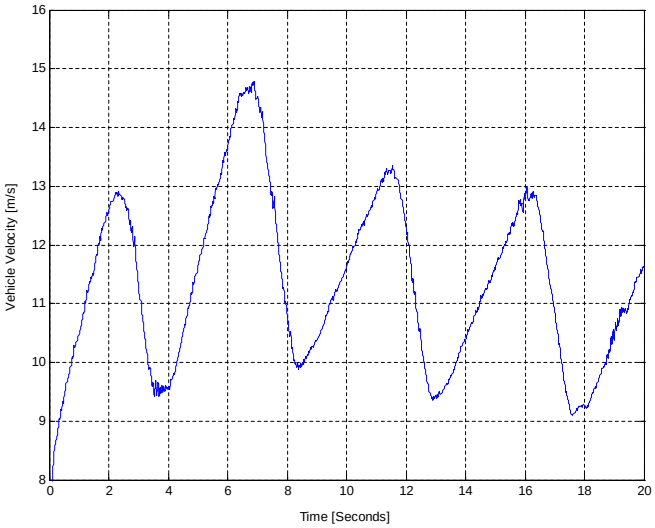

Figure 3.8: Velocity Profile for Normal Force Estimator

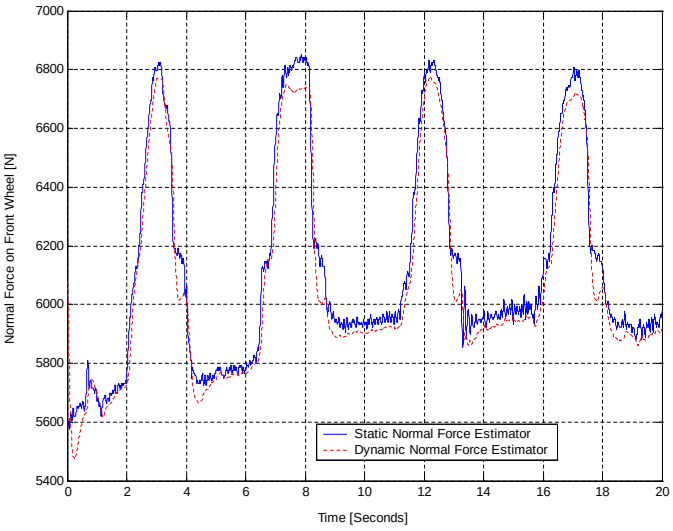

Figure 3.9: Normal Force on Front Wheel

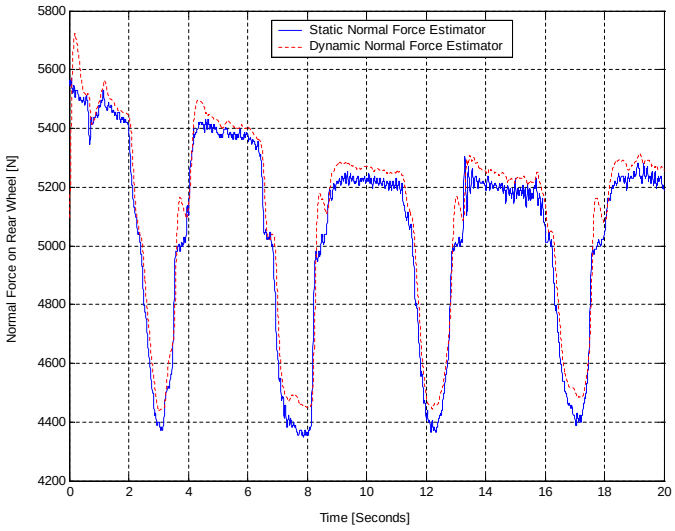

Figure 3.10: Normal Force on Rear Wheel

3.4 Tire Effective Radius Estimator

If the slip ratio is less than 0.05 in normal driving situation, it is very important to know the range of valid tire circumference. Specially, the tire circumference constantly changes depending on air pressure of the tire, speed, and normal force. Figure 3.11 shows the spring constant of the tire depending on the air pressure of the tire. Also, as shown in Figure 3.12, as the vehicle velocity increases, the circumferences of all four tires increase with the slope of 0.0004 [m/(m/s)].

Therefore, when normal force, vehicle speed, and tire pressure are considered, the amount of change in circumference of a tire can be shown in Equation 3.11.

$$\Delta R = \frac{F_{No} - k_v k_t v}{k_t F_{No}} \times F_N \tag{3.11}$$

Here, F_{No} is the initial normal force when the vehicle stops, and $F_N$is the actual normal force when the vehicle is in motion, and it is obtained from Normal Force Estimator. k_v is the velocity constant of tire (0.0004 [m/(m/s)]), k_t is the tire spring constant, and v is the velocity of the vehicle. However, the actual circumference when the vehicle is in motion is shown in

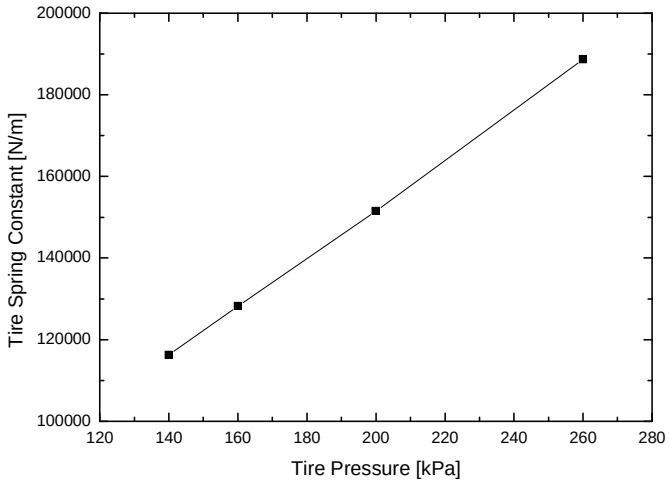

Figure 3.11: Tire Spring Constant Change with Tire Pressure

Equation 3.12.

$$R_e = R - \frac{1}{k_r}\Delta R \tag{3.12}$$

Here, k_r is constant value depending on tire and usually is the value of 3. Figure 3.13 shows the estimation of tire radius using Equation 3.11 and 3.12 under free rolling situation. and Figure 3.14 shows the effective radius estimation using the velocity profile of Figure 3.8

3.5 Road Force Estimation

With ordinary automotive sensor, road force applied to a tire cannot be observed. However, in this research a strain gauge is attached between the front left brake disk and the wheel to obtain brake torque, which occurs when braking. The dynamic equation of a wheel is shown as in Equation 3.13, and the road force applied on tire can be determined as in Equation 3.14.

$$J\dot{\omega} = -T_B - F_t r \tag{3.13}$$

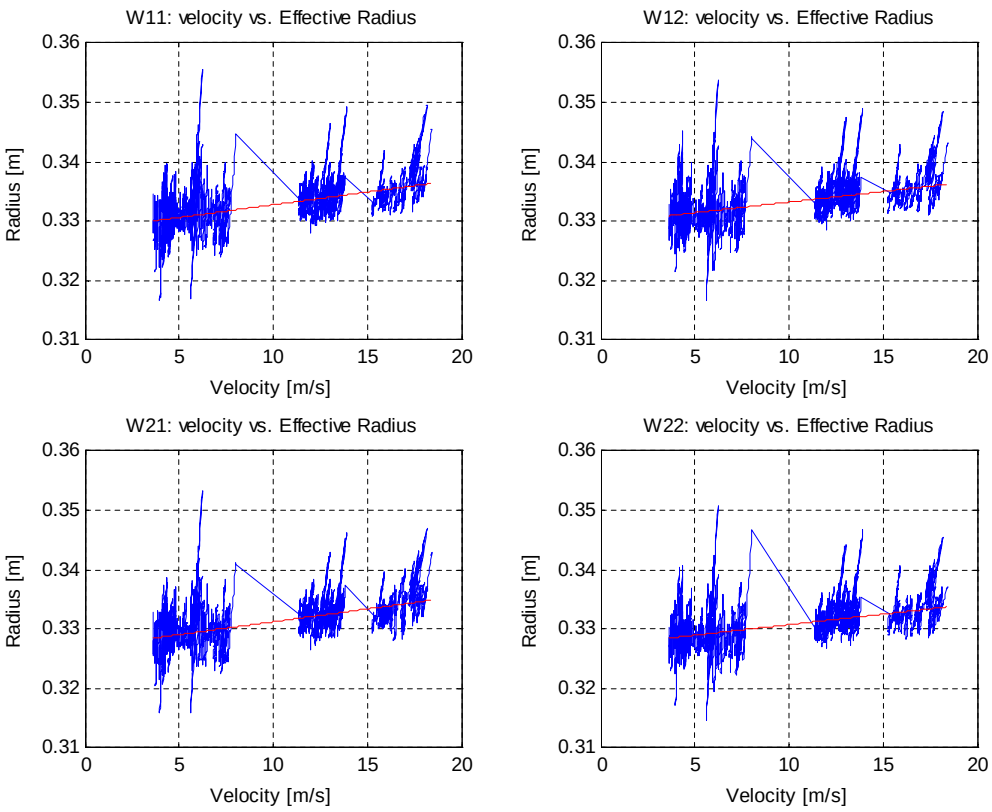

Figure 3.12: Tire Radius vs. Vehicle Speed

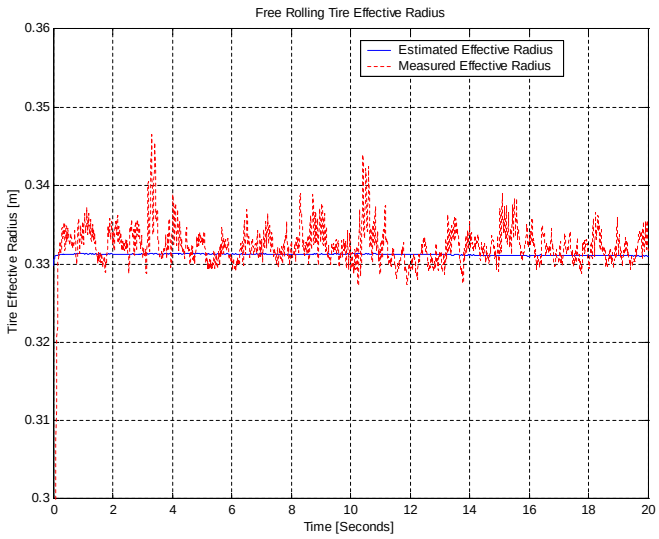

Figure 3.13: Effective Tire Radius Estimator under Free Rolling

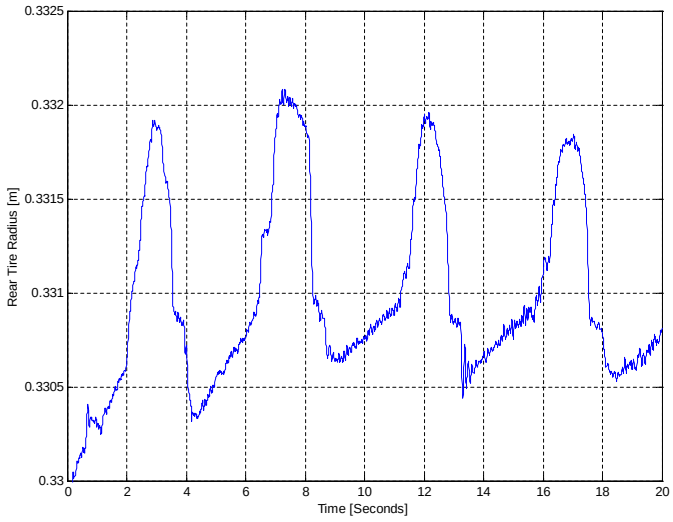

Figure 3.14: Effective Tire Radius Estimation

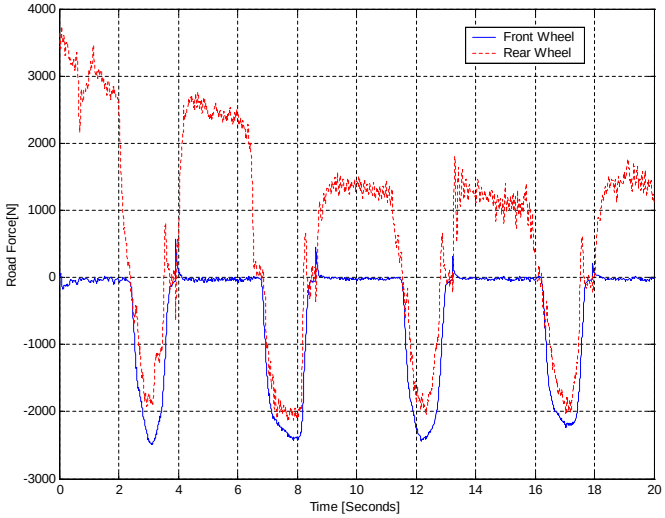

Figure 3.15: Road Force Estimation

$$F_t = \frac{(-T_B - J\dot{\omega})}{r} \tag{3.14}$$

Therefore, supposing the brake torques on front left wheel is same with that of front right wheel, the road force applied on front right wheel can be determined. Also, as vehicle dynamics equation is equivalent to Equation 3.16, road force applied on rear wheels can be found in Equation 3.16.

$$m\ddot{u_x} = -F_d - F_r + (F_{t11} + F_{t12} + F_{t21} + F_{t22}) \tag{3.15}$$

$$F_{t21} + F_{t22} = m\ddot{u_x} + F_d + F_r - (F_{t11} + F_{t12}) \tag{3.16}$$

Here, F_d, F_r represents drag force and rolling resistance, respectively. Figure 3.15 shows the road force estimation when the vehicle has the same velocity profile as in Figure 3.8.

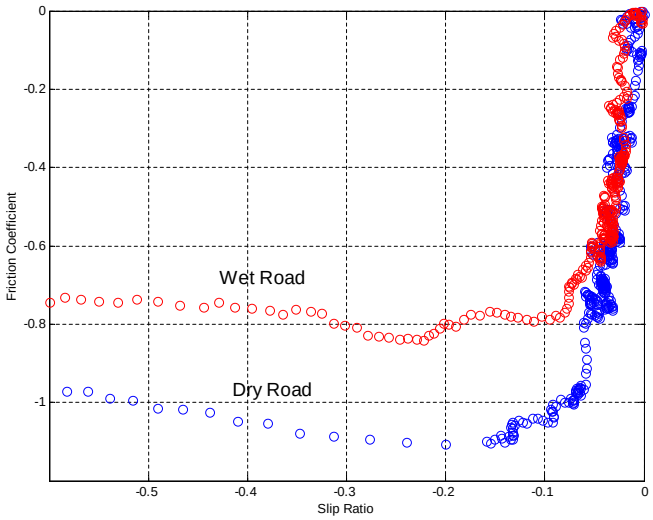

Figure 3.16: Slip Curve under different road condition

3.6 Slip Slope Detection for Maximum Friction Coefficient Estimation

It is widely known that depending on the road condition, the slope and even the maximum friction coefficient in slip vs. friction coefficient graph change. Therefore, under a certain value of slip, the slope is different depending on the characteristic of the road condition: dry, wet, snowy and icy. In this research, using the special behavior of slip that occurs when the brake pressure is linearly increased on dry and wet asphalt road, the full slip curve can be obtained as shown in Figure 3.16. In order to monitor the road condition using initially low slip, the slip within the range of -0.02 0.02 is used. As shown in Figure 3.17, slips on dry asphalt road and wet asphalt road are definitely different. Slip and friction coefficient have a linear relationship as shown in Equation 3.17, and using the linear regression method the slope can be found.

$$\mu = k \cdot s \tag{3.17}$$

Also, to monitor the road condition in real time, Recursive Least Square Estimation with the Forgetting Factor is used.

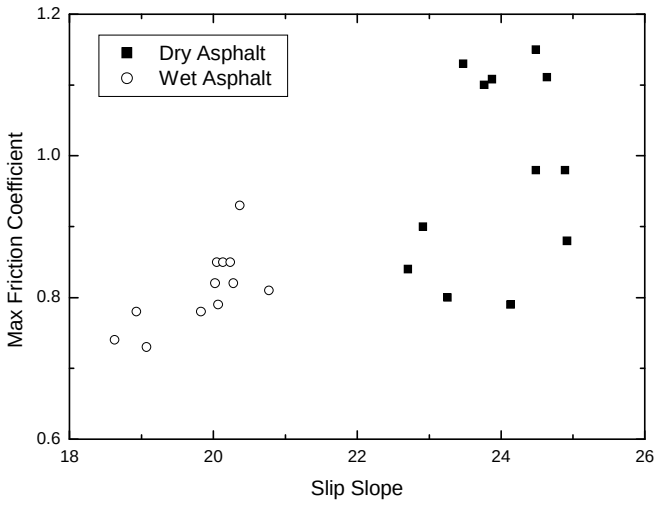

Figure 3.17: Maximum Friction Coefficients Distribution

$$y(k) = \theta\phi(k)^T \tag{3.18}$$

$$\hat{\theta}(k+1) = \hat{\theta}(k) + \frac{F(k)\phi(k) - \hat{\theta}(k)^T\phi(k)}{\lambda + \phi(k)^T F(k)\phi(k)} \tag{3.19}$$

$$F(k+1) = \frac{1}{\lambda}\left[F(k) - \frac{F(k)\phi^T(k)\phi(k)F(k)}{\lambda + \phi^T(k)F(k)\phi(k)}\right] \tag{3.20}$$

Here in these equations, F and λ are adaptive gain and forgetting factor, respectively. Using this method, Figure 3.18 and 3.19 express slip slope with varying forgetting factor when acceleration and deceleration repeatedly occur on dry and wet road.

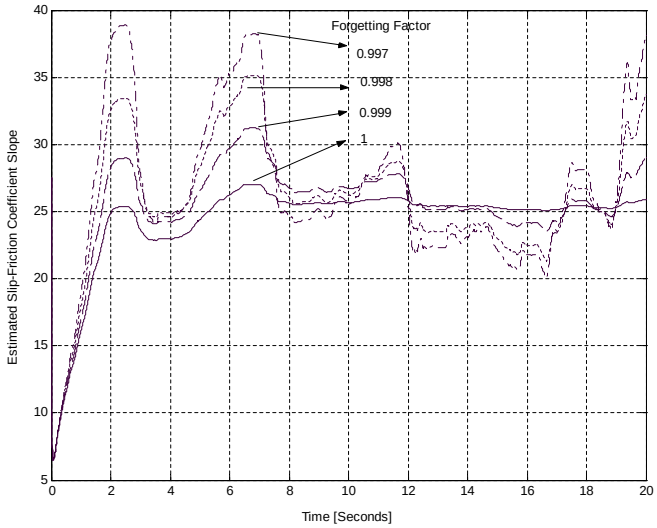

Figure 3.18: Slip Slope Estimation using Recursive Least Squares [Dry Road]

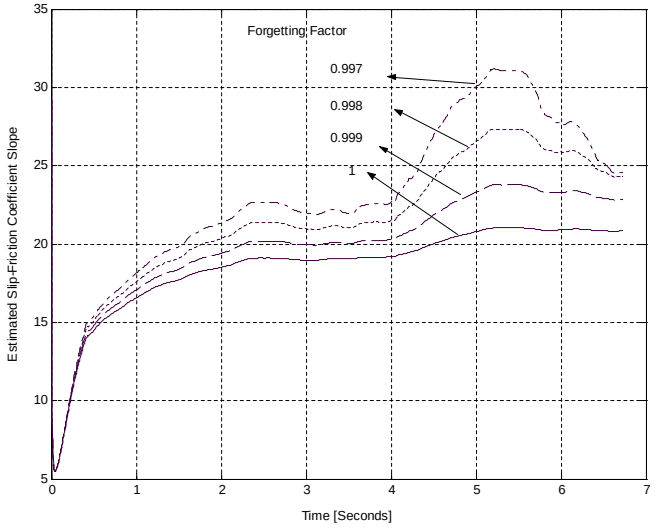

Figure 3.19: Slip Slope Estimation using Recursive Least Squares [Wet Road]

Chapter 4

Conclusion

1. In Chapter 1, we study the effect of vehicle-vehicle/roadside-vehicle communication on the performance of Adaptive Cruise Controlled (ACC) highway system. For the types of ACC applications we studied, V-V/V-R communication brings great benefits. The benefits can be observed in terms of efficiency (waiting-to-merge queue length), safety (shock wave, braking effort, etc.) and passenger's comfort (braking efforts). Simple communication concepts like location based broadcasting and intermediate communication could work very well in these applications, but for some applications such effects are not obvious. The simulation works can serve as the guideline for further experimental work. For example, the braking scenario and similar applications should not be the focus of future experiment. Besides the experiments, how to design protocol to realize such communication with high Qos, and low cost is another direction of future work.

2. In Chapter 2, a new vehicle longitudinal motion controller is suggested. The availability and the the performance of the controller is checked through simulation and compared with the previously used control method. A new method shows a better performance with smaller space tracking error than limited slip assumption controller in the simulation. However, the difficulty lies in measuring the precise slip data and heavy data handling for the implementation of the method. Also, the the fast slip dynamics are hard to catch using the current actuator with inevitable time delay. As a result, the new control strategy is not recommended with the existing level of technology.

Emergency braking maneuvers of the vehicle following the current control scheme of the longitudinal motion has been analyzed with experimental vehicle. Within the bounds of deceleration limits that the vehicle can follow the controller with the limited slip assumption showed good performance.

3. In Chapter 3, the primary task of this research is to accurately obtain the slip of a wheel. First, a fifth wheel is used to obtain the accurate velocity of the vehicle, and the angular velocity of each wheel is measured. To obtain the circumferential velocity, the exact tire radius is needed. The change in the spring constant based on tire air pressure is obtained, and also the increase in tire radius due to the faster velocity is considered. The normal force applied on each wheel due to the pitch motion resulting from acceleration and deceleration is estimated. Brake torque sensor and accelerometer are used to find the normal force. Using the estimated normal force and road force, the tire-road friction coefficient is obtained.

   Also, the slip-friction coefficient curves under two different road conditions, dry and wet, are examined. First, on two types of roads the brake pressure is linearly increased to obtain full slip curve, and the maximum friction coefficient is estimated. Also, under two types of road conditions, the different slopes of slip-friction coefficient are definitely distinguished from each other, having slip in the range -0.02–0.02. In actual driving situations, current road condition needs to be judged, and therefore, recursive least squares is used to obtain slip slope in real time.

   However, in order to obtain the maximum friction coefficient with the observed slip slope, an algorithm based on the brush model of a tire is needed. This research gives a foundation on emergency braking control by providing a method of maximum friction coefficient estimation.

Bibliography

[1] http://www.leearmstrong.com/dsrc/dsrchomeset.htm.

[2] http://www.path.berkeley.edu/shift/.

[3] K. Ahmed. *Moedling Driver's Acceleration and Lane Change Behavior*. PhD thesis, MIT, 1999.

[4] L. Alvarez and R. Horowitz. Hybrid controller design for safe maneuvering in the path ahs architecture. *Proceedings of the American Control Conference*, 1997.

[5] A. Bose and P. Ioannou. Analysis of traffic flow with mixed manual and semi-automated vehicles. Technical Report UCS-ITS-PRR-99-14, California PATH, 1999.

[6] L. Briesemeister and G. Hommel. Disseminating messages among highly mobile hosts based n inter-vehicle communication. *IEEE Intelligent Vehicle Symposium*, 2000.

[7] M. Cremer, C. Demir, S. Donikian, S. Espie, and M. McDonald. Investigating the impact of aicc concepts on the traffic flow quality. *Fifth World Congress on Intelligent Transportation Systems*, 1998.

[8] D. N. Godboyle and J. Lygeros. Safety and throughput analysis of automated highway systems. Technical Report UCB-ITS-PRR-2000-1, California PATH, 2000.

[9] J.K. Hedrick, D. Godbole, R. Rajamani, and P. Seiler. Stop and go cruise control final report. http://vehicle.me.berkeley.edu/Publications/AVC/pqixu_vtc02.ps.

[10] A. Kato, K. Sato, and M. Fujise. Wave propagation characteristics of inter-vehicle communication on an expressway. *Eigth World Congress on Intelligent Transportation Systems*, 2001.

[11] J. Lygeros and N. Lynch. Conditions for safe deceleration of strings of vehicles. Technical Report UCB-ITS-PRR-2000-2, California PATH, 2000.

[12] B. Song and D. Delorme. Human driver model for smartahs based on cognitive and control approach. *Proceedings of the 10th Annual Meeting of the Intelligent Transportation Society of America*, 2000.

[13] J. VanderWerf, N. Kourjanskaia, S. Shladover, H. Krishnan, and M. Miller. Modeling the effects of driver control assistance systems on traffic. *U.S. National Research Council Transportation Research Board 80th Annual Meeting*, January 2001.

[14] P. Zwaneveld and B. van Arem. Traffic efffects of automated vehicle guidance systems. *Fifth World Congress on Intelligent Transportation Systems*, October 1998.